Optical and Quantum Electronics (2020) 52:213
https://doi.org/10.1007/s11082-020-02337-1

Electron density transport using microring circuit for dual-mode power transmission

A. E. Arumona[1,2,3] · I. S. Amiri[1] · S. Punthawanunt[4] · K. Ray[5] · P. Yupapin[1,2]

Received: 27 December 2019 / Accepted: 30 March 2020

Abstract
The transport of electron density using silicon microring resonator arrangement proposed. A proposed system consists of a transmitter and a receiver, which can position with a distance away. The transmitter has a silicon microring with two nanoring phase modulators while the receiver has five silicon microrings with each having two-sided nanorings. A gold grating embedded at the center of the silicon microring, from which the plasmonic polariton induced by the coupling between the gold grating and incident light and leads to the plasmonic wave oscillation. In a simulation, the light source of 1.55 μm wavelength fed into the system and the input power varied from 1 to 10 mW for all calculations, the Bragg wavelength at resonant peaks applied for plasma frequency identification. The trapped electrons can transport to the required destination by the dual-mode transmission, wireless or cable connection. At resonance, the whispering gallery mode obtained by controlling the two nanoring phase modulators. The motivation of this work is the electron density can generate and transport within the microring system. The key finding is the successful transport of electron density in dual-mode using the silicon microring resonator arrangement, from which the gain amplifier also achieved. In application, the power transmission using the remote current source (charger) is possible.

Keywords Electron density · Electron transport · Silicon microring · Dual-mode transmission · Gold grating

✉ P. Yupapin
preecha.yupapin@tdtu.edu.vn

A. E. Arumona
arumonaarumonaedward.st@tdtu.edu.vn

[1] Computational Optics Research Group, Advanced Institute of Materials Science, Ton Duc Thang University, District 7, Ho Chi Minh City, Vietnam

[2] Faculty of Applied Sciences, Ton Duc Thang University, District 7, Ho Chi Minh City, Vietnam

[3] Division of Computational Physics, Institute for Computational Science, Ton Duc Thang University, Ho Chi Minh City 700000, Vietnam

[4] Faculty of Science and Technology, Kasem Bundit University, Bangkok 10250, Thailand

[5] Amity School of Applied Sciences, Amity University, Jaipur, Rajasthan, India

Published online: 05 April 2020

1 Introduction

Electron density measures the probability of an electron to be present at a given location. The higher the electron density in a given region, the higher the likelihood of an electron is being present in that region. In a many-electron system such as electronic and photonic devices, where the main macroscopic measurable is the electron density (Serebrennikov 2016; Zhu and Xu 2017; Tunsiri et al. 2019). Silicon microring circuit has many applications, where the ease in its fabrication and flexible applications makes it the choice of use by many researchers (Youplao et al. 2018; Singh et al. 2019; Pornsuwancharoen et al. 2017; Liou and Wang 2019; Li et al. 2016; Atabaki et al. 2018; Singh and Mandal 2019; Ali et al. 2018; Arumona et al. 2020). The advantage is that the panda-ring circuit which makes use of the silicon microring can apply as dual-mode operation, which can apply as a wireless connection and as well as a cable connection. The connection can apply in an optical fiber network, where the signals transmitted through the cable; for the wireless connection. The light fidelity (LiFi) network can employ easily in different ways using the concept of the whispering gallery mode (WGM) (Punthawanunt et al. 2018; Khomyuth et al. 2018). The whispering gallery mode is as a result of trapping of light inside a microring; this phenomenon is made possible due to the nonlinearity exhibited by the silicon microring circuit. The WGM phenomenon has been applied in different forms and used for various applications (Bunruangses et al. 2019; Trong and Chang 2017). In metals electron density oscillations give plasma waves; also the plasma wave properties depend on electron density. Denis and Nikolic (2010) studied the transport of electron density in the graphene nanoribbon device. The duo developed an algorithm by combining two efficient algorithms numerically; that is, the nonequilibrium Green function and density functional theory (DFT) were combined numerically and used for the study of electron density in this device. Ardaravičius et al. (2017) studied the electron density transport in doped ZnO; various deductions were made based on electron density transport within the doped ZnO material. McCreery et al. (2014) studied electron transport in electronic devices made up of carbon molecules. Rakoski et al. (2019) studied electron transport using the measuring methods of Van der and Shubnikov in N-polar GaN heterostructures. Wang et al. (2019) carried out an extensive study on the electron transport in $BaSnO_3$ films, where the electron mobility and mechanisms studied in great details. Anusha et al. (2019) studied electron transport in an electronic device made up of molecular nanometal using the plane wave scattering DFT. Toussaint et al. (2018) studied electron transport in mesoscopic networks, where the microscopic experiment applied for the study, where the results showed the electron density decreased the locally the mesoscopic network electrical conductance increased. Kornblum et al. (2015) studied electron transport in titanate heterostructures, where improvement on the electron transport properties of this heterostructures achieved and their results give insight on the possibility of creating high electron density devices such as oxide 2DEGs (2D electron gas) integration on Si. In this work, the transport of electron density using the silicon microring (Nagarajan et al. 2020; Wright et al. 2019) circuit is studied; the proposed system comprises the transmitter which has silicon microring at the center with two side nanorings and a receiver with five silicon microring with each having two nanorings at their sides. The Optiwave program employed to study the system leading to the formation of whispering gallery modes that have the advantage of the dual-mode operations, which are (1) wireless link called light fidelity (LiFi) network and (2) the cable network via the fiber-optic network.

For simplicity, the used parameters extracted from the Optiwave program will be used in the MATLAB program for the transport of electron density from the transmitter to the receiver.

2 Background

The silicon microring system embedded gold gratings at the center of the microrings. The electrons in the metal (gold grating) intersected with the incident light described by the Drude model (Tunsiri et al. 2019). The induced plasma frequency and electron density are given by the Drude model in an Eq. (1).

$$\epsilon(\omega) = 1 - \frac{\mathrm{ne}^2}{\epsilon_0 \mathrm{m}\omega^2} \tag{1}$$

where n is the electron density, ϵ_0 is the relative permittivity, m is the electron mass, e is electron charge, and ω is the angular frequency. The plasma frequency (ω_p) at the resonance is given by

$$\omega_\mathrm{p} = \left[\frac{\mathrm{ne}^2}{\epsilon_0 \mathrm{m}}\right]^{-1/2} \tag{2}$$

From Eq. (2), the electron density, $n = \frac{\omega_p^2 \in_o m}{e^2}$. The plasmonic wave oscillation is as a result of electron density in an electric field. The TM- polarization along with exponential decay of the electric field is obtained by Maxwell's equations. The electric field fed into the system given by an Eq. (3) (Youplao et al. 2018).

$$E_Z = E_0 e^{-ik_z z - \omega t} \tag{3}$$

where E_0 is the initial electric field amplitude, the wave vector in the z-axis direction is $k_z = \frac{2\pi}{\lambda}$, the input light source wavelength is λ. The angular frequency is $\omega = 2\pi\gamma$, where γ is the linear frequency, and time is t. The wavelength at resonance related to the Bragg wavelength as follows $\lambda_B = 2\ 2n_e\wedge$. The effective refractive index is n_e, which represents the grating's refractive index in the waveguide and the grating period is $\wedge$. The Kerr effect is a nonlinear effect, which determined by $n = n_0 + n_2 \mathrm{I} = n_0 + n_0 P/A_{eff}$, where the linear and nonlinear refractive indices are n_0 and n_2 respectively. The optical intensity and power are I and P respectively. The effective mode core area of the device is A_{eff}. The output fields of the silicon microring circuit are shown in Fig. 1, from which the relationship of the circuit ports described by the following equations (Suresh et al. 2015).

$$E_{th} = m_2 E_{in} + m_3 E_{add} \tag{4}$$

$$E_{drop} = m_5 E_{add} + m_6 E_{in} \tag{5}$$

where m_i and the related terms are the constants and found in the given references. E_{th}, E_{drop}, E_{add} and E_{in} are the throughput, drop, add and input ports, respectively. The whispering gallery mode of the Panda-ring can be controlled by the two side rings (phase modulators) at the resonant values, from which the normalized intensity at the throughput and drop ports obtained. The normalized output intensities are given by

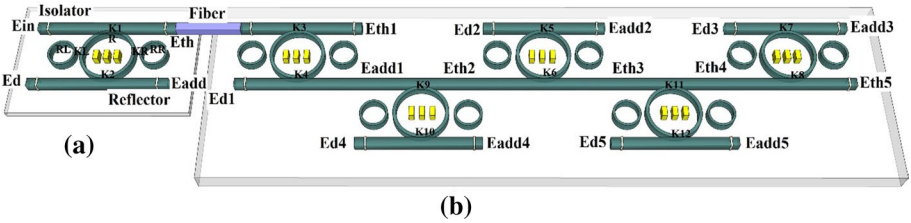

Fig. 1 The schematic of the system, where **a** the transmission part, **b** the receiver nodes. E_{in}: input port, E_{th}: throughput port, E_d: drop port, E_{add}: add port, R: main ring radius, R_L and R_R: left and right side ring radii, KL and KR: left and right ring coupling constants

$$\frac{I_{th}}{I_{in}} = \left[\frac{E_{th}}{E_{in}}\right]^2 \tag{6}$$

$$\frac{I_{drop}}{I_{in}} = \left[\frac{E_{drop}}{E_{in}}\right]^2 \tag{7}$$

In a simulation, the required output obtained by the suitably selected parameters of the Optiwave program. By using the Eqs. (1)–(7), all required outputs obtained and plotted using the MATLAB program.

3 Results and discussion

The simulation employed by the proposed system shown in Fig. 1, where Fig. 1a, b is the transmitter and receiver, respectively. The microring embedded gold grating is applied to form to excite the electrons on the gold grating surface by the WGM, where the plasmonic antenna can perform (Arumona et al. 2020). From which the trapped electrons can transport either by light (Wright et al. 2019) or electromagnetic waves (Youplao et al. 2018) have been recently reported. The trapped electrons can transmit and detect at the receivers shown in Fig. 1, where the results show in Figs. 2, 3 and 4. The input light source has a wavelength of 1.55 μm fed into the system through the input port. The resonant WGM excites the gold grating and leads to the oscillation of plasmonic waves (polaritons) at the Bragg wavelength. The whispering gallery mode (WGM) formed as a result of light coupling into the microring and gold grating at the center of the silicon microring; the gold grating usually shifts the input wavelength to the Bragg wavelength. The other output signals usually obtained from the throughput and drop ports. Firstly in manipulation, the Optiwave FDTD 32 bit version 12.0 (http://www.optiwave.com) employed and at resonance, where the light trapped inside the microring at a particular wavelength. The grid size used is 0.045 for Δx, Δy, and Δz respectively; the anisotropic perfect matched layer (APML) is used as the boundary condition, in which the number of AMPL layer is 15 with theoretical reflection coefficient of 1.0×10^{-12} and real tensor APML parameter of 1, the whole dimension simulation model has 661 mesh cell size in the x-axis, 55 mesh cell size in the y-axis and 1654 mesh cell size in the z-axis. To confirm the resonant results, the number of round trips was 20,000. For all simulations, the 32 GB RAM high-performance computer applied. By using the other selected

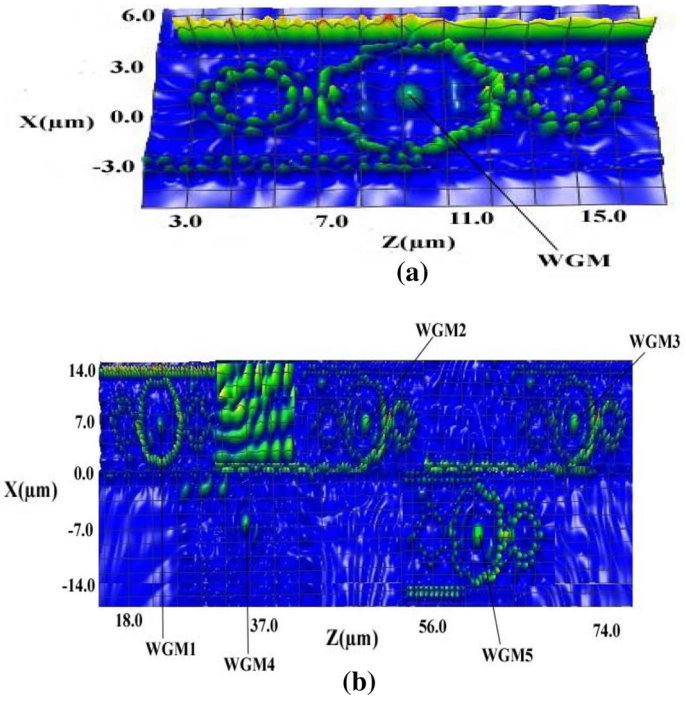

Fig. 2 The plot of the graphical results, where the input power is 10 mW with a center wavelength of 1.55 μm, the other parameters given in Table 1, where **a** the transmitter and **b** five receivers, where the different location of users applied

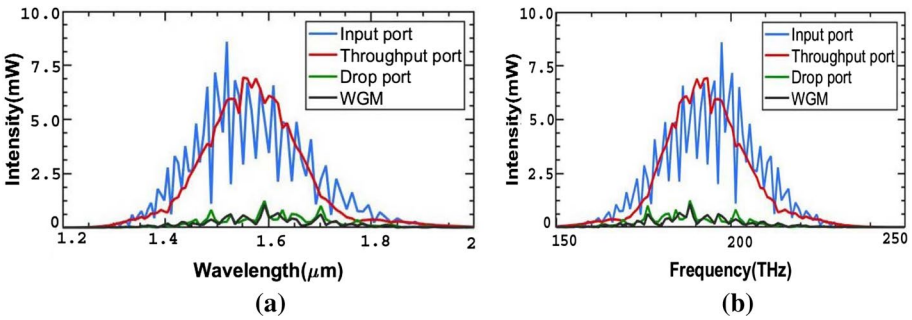

Fig. 3 The plot of the output and input intensity relationship using Fig. 2a, where **a** wavelength and **b** frequency domains. The Bragg wavelength output is at 1.59 μm, which shifted from the input wavelength at 1.55 μm

parameters, in Table 1, the required WGM outputs are obtained and shown in Fig. 2. They observed at the center wavelengths, where the shifted wavelengths (Bragg wavelengths) obtained and apply for plasma frequency calculation. From Fig. 2a the WGM formed at the center of the silicon microring with two-sided nanorings. In Fig. 2b, the WGM formed at the center of the receiver silicon microrings, with controlled by the two side nanorings. The plot of the relationship between the output intensity in wavelength

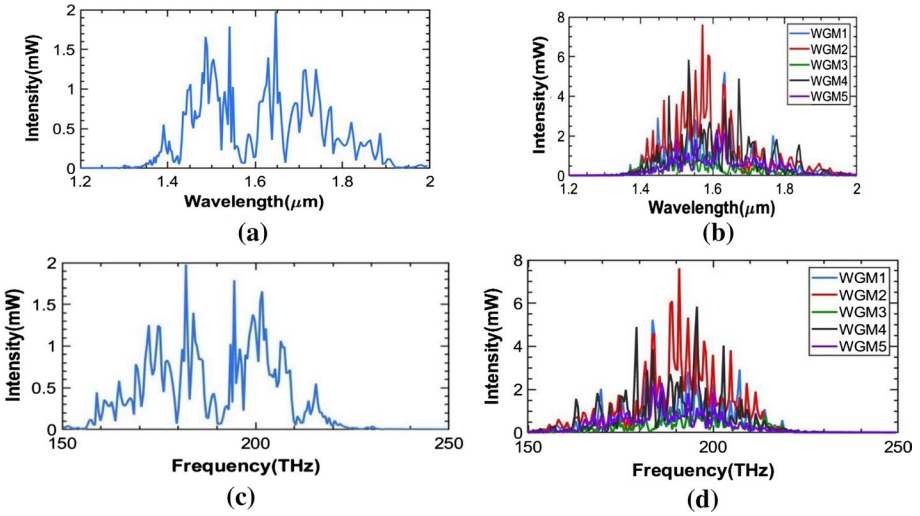

Fig. 4 The plot of the WGM outputs, where **a** transmitter in wavelength domain, **b** receiver in wavelength domain, **c** transmitter in frequency domain, **d** receiver in the frequency domain of the result in Fig. 2a, b. The Bragg wavelength result of the transmitter is at 1.65 μm, while for the receiver wavelength is at 1.59 μm, which shifted from the input wavelength at 1.55 μm

Table 1 The selected parameters of the system used in the simulation

Parameters	Symbols	Values	Units
Input power (Gaussian pulse)	P	1–10	mW
Si-linear waveguide length	L	16.0	μm
Si center ring radius	R	2.0	μm
Si small ring radius	R_L	1.0	μm
Si small ring radius	R_R	1.0	μm
Gold dielectric constant (Pornsuwancharoen et al. 2017)	ϵ_o	6.9	
Gold permittivity (Pornsuwancharoen et al. 2017)	ϵ	10.0	
Gold thickness	d	0.1	μm
Gold length	L	0.5	μm
Gold refractive index (Pornsuwancharoen et al. 2017)	n	1.80	
Coupling coefficient	κ	0.50	
Insertion loss	γ	0.01	
Refractive index Si (Prabhu et al. 2010)	n_{Si}	3.42	
Si nonlinear refractive index (Prabhu et al. 2010)	n_2	1.3×10^{-13}	m^2W^{-1}
Input light wavelength input port	λ_1	1.55	μm
Waveguide core effective (Prabhu et al. 2010)	A_{eff}	0.30	μm^2
Waveguide loss	α	0.50	dB (cm^{-1})
Fiber loss	–	0.10	dB km^{-1}
Plasma frequency (Blaber et al. 2009)	ω_p	1.2990×10^{16}	$radsec^{-1}$
Electron mass	m	9.11×10^{-31}	kg
Electron charge	e	1.6×10^{-19}	Coulomb
Permittivity of free space	ϵ_o	8.85×10^{-12}	Fm^{-1}

and frequency domains is shown in Fig. 3, where the center wavelength of 1.55 μm shifts to the Bragg wavelength of 1.59 μm. The parameters extracted from the Optiwave FDTD program applied in the MATLAB program and plotted the WGM in Fig. 4. The relationship of the electron density with the input intensity is shown in Fig. 5. From Fig. 4, the plot of the whispering gallery mode (WGM) is shown in Fig. 4a, b, which is the wavelength domain result. The transmitter center wavelength shifted from 1.55 to 1.65 μm, while the receiver center wavelength shifts from 1.55 to 1.59 μm. Figure 4c, d is the WGM of the transmitter and receiver in the frequency domain. Using Eqs. (6)-(7) and $n = \frac{\omega_p^2 \epsilon_o m}{e^2}$ from Fig. 5a, which shows the plot of the relationship between the electron density, throughput, drop ports and normalized intensity of the transmitter. Figure 5b shows the plot of the relationship between the electron density, drop ports and normalized intensity of the receiver. Figure 5c plots of the electron density, whispering gallery modes (WGMs) normalized intensity of the receiver. The result in Fig. 5 shows a linear trend as the power is varied from 1 to 10 mW. The electron density increases with increased power, which means that the amplified electron density obtained. The plot of the throughput and drop ports of the transmitter and receiver with varied input power 1–10 mW shown in Fig. 6. In applications, the dual-mode electron density transport can apply by wireless and cable connections, where the wireless can link by the short-range light fidelity (LiFi) network via the WGM output, while the cable connection can apply to the link via the optical fiber connection. However, in practice, the transmission loss in either via free-space or cable connection must be included. Moreover, the WGM output of the coupling grating having the antenna propagation profile (Arumona et al. 2020), which means that apart from the direct WGM beam transmission, the antenna transmission can also be applied.

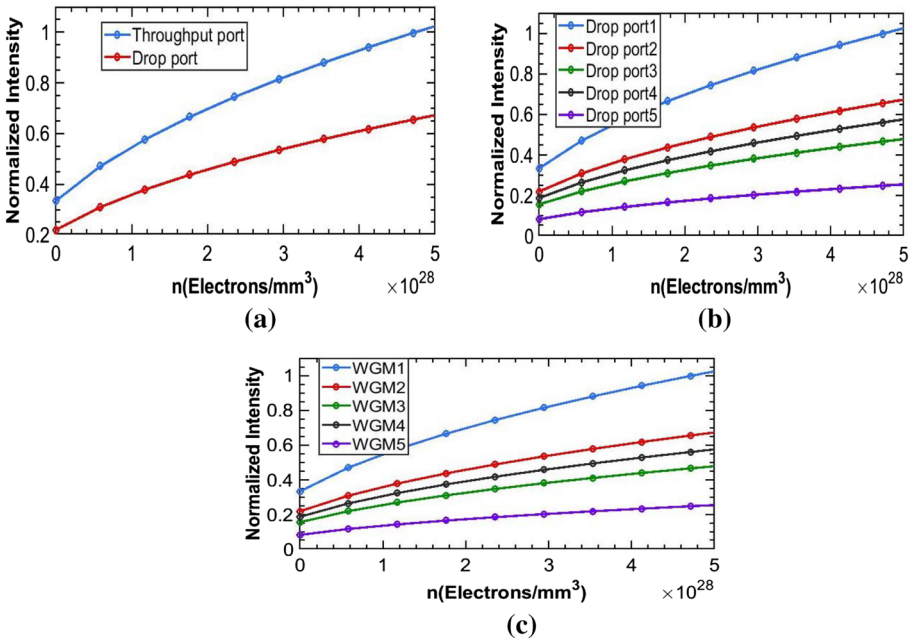

Fig. 5 The plot of the electron density, where **a** transmitter throughput and drop ports, **b** receiver drop ports, **c** the receiver whispering gallery modes

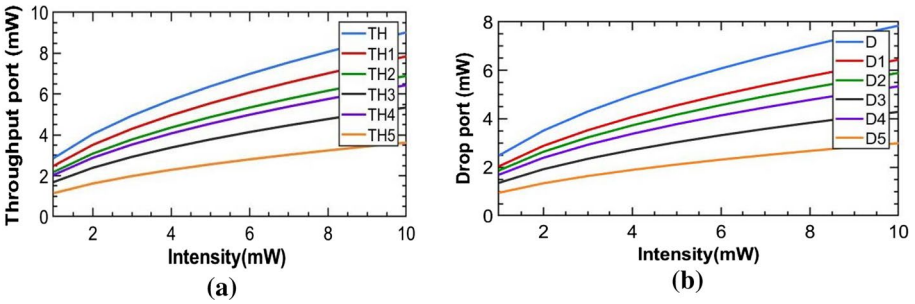

Fig. 6 The plot of the ratio of the electron densities for all nodes **a** Throughput port/Input signal for all nodes, **b** Drop port/Input port. The amplified output electron densities achieved

4 Conclusion

The transport of electron density using a silicon microring circuit proposed, where the simulation results have shown the promising results confirmed. This work has demonstrated the transport of electron density from the transmitter to the receiver by dual-mode, which is available for the new technique of power transmission without copper cable. The dual-mode can employ by cable connection through the device ports and wireless connection through the whispering gallery mode (WGM), where the electro-optic signal conversion can achieve by the dielectric-metal application. The dual-mode can apply by the cable connection through the device ports and wireless connection through the whispering gallery mode (WGM). The proposed work can give the advantages, which are (1) the electro-optic signal conversion and (2) the wireless-optical fiber connection can offer the dual-mode transmission. Regarding the selected material and parameters, such a circuit can be fabricated and applied. Moreover, the electron density transport can offer the use of the electron spin for spin electronics, quantum sensors, the electron spin transport, quantum computing device and signal processing. The plasmonic antenna formed by the proposed system is also available for antenna propagation based-on electron spin distribution, which will be the continuous work.

Acknowledgements One of the authors (Mr. Arumona) would like to thank the Ton DucThang University, Vietnam for their financial support.

References

Ali, J., et al.: Coherent light squeezing states within a modified microring system. Res. Phys. **9**, 211–214 (2018)

Anusha, V., et al.: Electronic transport in metal-molecular nanoelectronic networks: a density functional theory study. AIP Adv. **9**(3), 035122 (2019)

Ardaravičius, L., et al.: High-field electron transport in doped ZnO. Mater. Res. Express **4**(6), 1–6 (2017)

Arumona, A.E., Amiri, I.S., Yupapin, P.: Plasmonic Micro-antenna characteristics using gold grating embedded panda-ring circuit. Plasmonics **15**, 279–285 (2020)

Atabaki, A.H., et al.: Integrating photonics with silicon nanoelectronics for next generation of system on a chip. Nature **556**, 349–354 (2018)

Blaber, M.G., Arnold, M.D., Ford, M.J.: Search for the ideal plasmonic nanoshell: the effects of surface scattering and alternatives to gold and silver. J. Phys. Chem. C **113**, 3041–3045 (2009)
Bunruangses, M., et al.: Brain sensor and communication model using plasmonic microring antenna network. Opt. Quantum Electron. **51**(349), 1–10 (2019)
Denis, A., Nikolic, B.K.: Electron density and transport in top-gated graphene nanoribbon devices: first-principles Green function algorithms for systems containing a large number of atoms. Phys. Rev. B **81**(15), 155450 (2010)
Khomyuth, C., Mahdi, B., Amiri, I.S., Youplao, P., Pornsuwancharoen, N., Yupapin, P.: Electric-optic conversion circuit incorporating a fiber optic loop for light fidelity up-down link use. Microw. Opt. Technol. Lett. **61**(2), 526–531 (2018)
Kornblum, L., et al.: Electronic transport of titanate heterostructures and their potential as channels on (001) Si. J. Appl. Phys. **118**(10), 1–6 (2015)
Li, C., et al.: Silicon-microring-based thermos-optic non-blocking four port optical router for optical networks-on-chip. Opt. Quantum Electron. **48**(552), 1–22 (2016)
Liou, J., Wang, F.: Design and fabrication of ring resonator spectral response through-drop wavelengths selective. Opt. Quantum Electron. **51**(101), 1–11 (2019)
McCreery, R., et al.: Electron transport in all-carbon molecular electronic devices. Faraday Discuss. **172**, 9–25 (2014)
Nagarajan, A., et al.: Ultra-narrowband polarization insensitive transmission filter using a coupled dielectric-metal metasurface. Opt. Express **20**, 773–787 (2020)
OptiFDTD Technical Background and Tutorials (Finite Difference Time Domain Photonics Simulation Software, Version 12.0. http://www.optiwave.com
Pornsuwancharoen, N., et al.: Micro-current source generated by a WGM of light within a stacked silicon-graphene-Au waveguide. IEEE Photonics Technol. Lett. **29**(21), 1768–1771 (2017)
Prabhu, A.M., et al.: Extreme miniaturization of silicon add–drop microring filters for VLSI photonics applications". IEEE Photonics J. **2**(3), 436–444 (2010)
Punthawanunt, S., Aziz, M.S., Phatharacorn, P., Chiangga, S., Ali, J., Yupapin, P.: LiFi cross-connection node model using whispering gallery mode of light in a microring resonator. Microsyst. Technol. **24**(12), 4833–4838 (2018)
Rakoski, A., et al.: Electron transport in N-polar GaN-based heterostructures. Appl. Phys. Lett. **114**(16), 162102 (2019)
Serebrennikov, A.M.: On the estimation of density of collectivized electrons in plasmonic spherical metal nanoparticles: quantum static versus classical dynamic approach. Opt. Quantum Electron. **48**(376), 1–25 (2016)
Singh, K., Mandal, S.: Design and performance analysis of all-optical 1:4 and 1:8 high speed demultiplexer using InGaAsP-InP optical microring resonator in Z-domain. Opt. Quantum Electron. **51**(252), 1–26 (2019)
Singh, R., et al.: Parametric optimization of fiber to waveguide coupler using Bragg gratings. Opt. Quantum Electron. **51**(256), 1–10 (2019)
Suresh, N., et al.: Study of plasmonic resonance of gold through refractive index. J. Mater. Sci. Eng. **4**(1), 1–3 (2015)
Toussaint, S., et al.: On the origins of transport inefficiencies in mesoscopic networks. Sci. Rep. **8**(3017), 1–11 (2018)
Trong, H.B.N., Chang, Y.C.: Whispering gallery modes in hybrid Au-ZnO microsphere resonators: experimental and theoretical investigations. Opt. Mater. Express **7**(8), 2962–2967 (2017)
Tunsiri, S., et al.: Microring switching control using plasmonic ring resonator circuits for super-channel use. Plasmonics **14**, 1669–1677 (2019)
Wang, H., et al.: Wide-voltage-window reversible control of electronic transport in electrolyte-gated epitaxial $BaSnO_3$. Phys. Rev. Mater. **3**(7), 075001 (2019)
Wright, S.C., et al.: Microwave trap for atoms and molecules. Phys. Rev. Res. **1**, 033035 (2019)
Youplao, P., et al.: Microring stereo sensors model using KerrVernier effect for bio-cell sensor and communication. Nano Commun. Netw. **17**, 30–35 (2018)
Zhu, J., Xu, W.: Hybrid surface plasmon waveguide device of periodic grating structure. Opt. Quantum Electron. **49**(351), 1–11 (2017)